Phase and Energy Relaxation of Vibrational Motion and Its Manifestation in Femtosecond Pump−Probe Experiments on I_2 in Rare Gas Environments

V. A. Ermoshin and V. Engel*

Institut für Physikalische Chemie, Universität Würzburg Am Hubland, 97074 Würzburg, Germany

A. K. Kazansky

Fock Institute of Physics, The University of St. Petersburg, 198504 St. Petersburg, Russia

Received: December 7, 2000; In Final Form: March 26, 2001

We present a classical description of femtosecond time-resolved experiments on collision-induced vibrational relaxation processes. For I_2 embedded in Ar and He gases, a hot distribution of molecular vibrational states is prepared by a pump laser pulse. Collisions of I_2 with gas atoms lead to dephasing and energy relaxation in the vibrational degree-of-freedom. In employing energy-phase coordinates, we are able to separate these two effects. Decay rates as obtained from the Fourier analysis of pump−probe signals are compared to those derived from the coordinate autocorrelation-function. It is shown that the vibrational energy relaxation influences the decay of the oscillatory structure in transient signals, leading to a nontrivial density dependence of the dephasing rate as observed in the experiments of Liu et al. [*J. Phys. Chem.* **1996**, *100*, 18650].

1. Introduction

Femtosecond time-resolved experiments aim at the investigation of dynamical processes in real time;[1−4] for recent reviews see, e.g., refs 5 and 6. The I_2 molecule has been a model system to monitor bound state rovibrational dynamics in the gas phase[7−10] and has also been used to demonstrate fundamental concepts and test new technologies.[11−18] The iodine molecule has also been used to study the elementary problem of an anharmonic oscillator coupled to its surroundings. For example, several femtosecond studies have been devoted to the dynamics of I_2 in cryogenic matrices[19,20] and zeolites.[21] Furthermore, Zewail and co-workers have performed pump−probe experiments on I_2 in various rare-gas surroundings.[22−24] In these studies, the systematic change of the pressure conditions allowed for a characterization of processes such as relaxation and predissociation. Also, the famous cage effect,[25] induced by single-atom collisions, was demonstrated using femtosecond spectroscopy.[26]

For the isolated I_2 molecule it is possible to apply quantum theory for a description of the molecular system interacting with femtosecond pulses. It is obvious that a complete quantum mechanical treatment of complex system−bath interactions is not feasible so that, if a theoretical description is wanted, one is forced to employ approximations. It is a major task to review the various methods used in the description of femtosecond spectroscopy; this has already been done in the excellent review article by Manz[27] to which we refer at this point.

In a former work[28] we adopted a mixed classical/quantum approach to simulate pump−probe experiments on iodine in rare gases. In employing a mean field approach we found that at longer times and especially at higher pressures the mixed description becomes inconsistent, which is not true for the classical calculation. A complete classical description of pump−probe experiments has been employed by various authors.[29−32] For a classical description of nonlinear coherent femtosecond experiments see, e.g., refs 33 and 34, and for recent interesting applications mixing quantum chemical methods with molecular dynamics (MD) see the work of Hartmann et al.[35,36]

Most of the latter theoretical work starts with a density-matrix formulation of the problem, as discussed extensively in the book by Mukamel.[37] Recently, we approached the problem of a classical description of coherent excitation processes starting with the wave function formulation of quantum mechanics.[38] We showed that, using the Wigner transformation,[39] the recipe to describe laser excitation can be derived in a straightforward manner. Furthermore, a comparison of quantum and classical calculations of pump−probe fluorescence signals (using again the I_2 molecule as a numerical example) revealed that the classical approximation yields reliable results. In the present paper, we apply classical mechanics to study the effect of an environment on the internal motion of iodine molecules and its manifestation in femtosecond time-resolved signals.

Figure 1 illustrates a pump−probe experiment on gas-phase iodine molecules. Here a first laser pulse prepares a vibrational wave packet which oscillates within the potential well of the electronic B state. The time-delayed probe pulse induces a transition to a higher electronic state. The probe wavelength may be chosen differently, as indicated by the different arrows in the figure. Measurement of the total fluorescence signal as a function of delay time yields information about the vibrational dynamics.[8]

Upon I_2 collisions with surrounding atoms, the internal vibrational energy changes (energy relaxation) and a phase randomization occurs (dephasing). In a recent preliminary study we showed that, by using energy and phase coordinates, the effect of energy relaxation and dephasing can be decoupled.[40] Here we elaborate the latter model, thereby extending earlier classical studies of I_2 dynamics in rare-gas environments.[23] In performing molecular dynamics simulations we show that the vibrational dynamics in "energy-phase" coordinates yields a transparent physical picture of collision-induced vibrational relaxation and allows for the separation of energy- and phase-

10.1021/jp004408u CCC: $20.00
Published on Web 07/20/2001

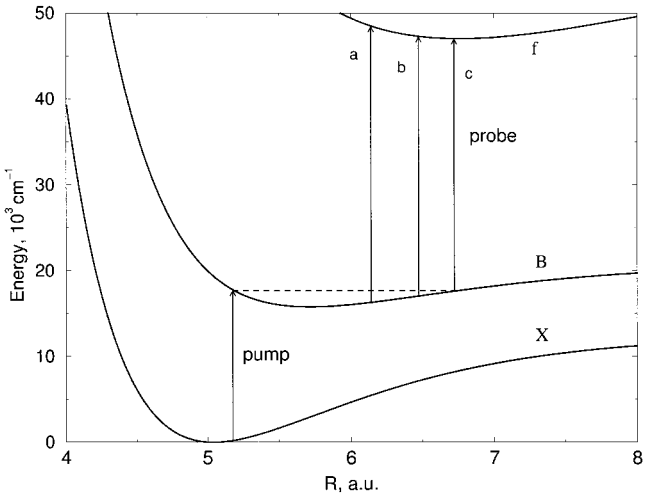

Figure 1. Pump−probe excitation scheme for gas-phase I_2 molecules. Shown are potentials corresponding to the ground (X), an excited (B), and an ion-pair electronic state (f), from which fluorescence is detected. The arrows indicate the center wavelengths of the pump (620 nm) and probe (280 nm (a), 310 nm (b), 330 nm (c)) femtosecond pulses.

relaxation processes. Moreover, we calculate pump−probe signals that can be directly compared to experiment.

This paper is organized as follows: the computational scheme is described in section 2. Section 3 contains the numerical results, and a discussion including a summary is given in section 4.

2. Molecular Dynamics Calculations

The molecular dynamics (MD) calculation employed a box containing one I_2 molecule surrounded by 124 Ar (He) atoms. Periodic boundary conditions were applied, and the size of the MD box, which was chosen according to the rare gas density, varied up to 20 nm^{-3}; a relation to the pressure can be found in ref 22. All simulations have been carried out at a temperature $T = 300$ K, which corresponds to the experimental conditions reported in ref 23. The set of Newtonian equations has been integrated with the velocity Verlet algorithm.[41] The numerical results, as reported here, result from an average over 10^4 trajectories. During the first picosecond of each run, the system was equilibrated by scaling the velocities of the ambient gas molecules with a relaxation constant of 0.4 ps.[41] After this time, the pump−pulse excitation process from the electronic ground state X to the electronic B state proceeds, as described below.

The potential-energy curves for the electronic X and f states of I_2 were taken from refs 42 and 43. The B state Morse parameters have been set to $D = 5103.1$ cm^{-1}, $\alpha = 0.9033$ au, and $r_0 = 5.711$ au as a result of a fitting of the potential given in ref 42 in an interval between 5.3 au and 6.5 au of the I−I distances. This is the region accessible by the B state wave packet prepared in the pump process at a center wavelength of 620 nm. The I_2−He and I_2−Ar potentials have been represented by a sum of atom−atom potentials with Morse functional form and parameters from refs 44 and 45. The parameters of the Lennard-Jones parametrization for the He−He and Ar−Ar interactions have been taken to reproduce the equilibrium distance and well depth of more sophisticated Hartree−Fock dispersion potentials from ref 46 and ref 47, respectively. To avoid problems arising at the bounds of the MD box, we have used the "shifted force" potentials with a cutoff distance $R_{cut} = 7$ Å.[41]

The vibrational wave packet, prepared in the pump process, is represented by a swarm of classical trajectories sampled from the function (atomic units are used throughout)

$$\rho_B(R_0, P_0, t_0) = e^{-E(R_0,P_0)/k_BT}\, e^{-\tau^2 D_{pu}^2(R_0)}\, e^{-t_0^2/\tau^2} \qquad (1)$$

This distribution of initial coordinates R_0 and momenta P_0 is a product of three exponential functions. The first one gives the Boltzmann distribution of classical particles with energies $E(R_0, P_0) = U_X(R_0) + P_0^2/2m$ at a temperature T. Here m is the I_2 reduced mass and U_X the ground-state potential. The second exponential in eq 1 defines the Franck−Condon window for the pump transition. The latter is obtained as the Fourier transform of the pump−pulse temporal shape function with respect to the function $D_{pu}(R) = U_B(R) - U_X(R) - \omega_{pu}$.[48−50] Here U_X and U_B are the potentials of the two electronic states that are involved in the transition, and ω_{pu} is the carrier frequency of the pump−pulse. The last exponential function appearing in eq 1 contains the pulse-shape function $f(\sqrt{2}t)$, which we choose to be a Gaussian $f(t) = \exp(-t^2/2\tau^2)$. It accounts for the probability of the molecular excitation at time t_0 during the pump process. The parameter τ was chosen such that the width (full-width-at-half-maximum, fwhm) of the electric field intensity of the pump pulse is 60 fs.

The classical description of the laser excitation is similar to its quantum mechanical counterpart, where the excited-state wave function is built by a coherent superposition of the initial (ground state) wave function promoted to the excited state at different times with different phases and weights.[51] A comparison of the classical distribution function with the quantum Wigner function describing the system after the pulse excitation reveals similar features.[38] As expected, the classical approximation becomes better with decreasing pulse width. Although the nodal structure of the wave function is not present in the classical density, the coordinate and momentum distribution of both the functions agree, in the average, very well.

The fluorescence signal from the ion-pair state is assumed to be proportional to the population of this state created in the probe transition. Dropping unimportant constants, the latter can be approximated as[52]

$$S(t_d) = \int dt\, f(\sqrt{2}(t - t_d)) \frac{1}{N} \sum_i^N F(R_i(t)) \qquad (2)$$

where the sum runs over the number N of initial configurations of the I_2/Ar system. Thus $S(t_d)$ counts the I_2 vibrational trajectories located within a spatial window defined by the weight function

$$F(R) = \exp(-\tau^2 (D(R) - \omega_{pr})^2) \qquad (3)$$

Here $D(R) = U_f(R) - U_B(R)$ is the difference between the f- and B-state potential, and ω_{pr} is the probe−pulse frequency. Note that eq 2 also contains the probe−pulse shape function centered at the delay time t_d between the pump and probe pulses. We note that the quantum mechanical version of eq 2, which reads

$$S(t_d) = \int dt\, f(\sqrt{2}(t - t_d)) \int dR\, |\psi_B(R, t)|^2 F(R) \qquad (4)$$

is the best approximation to the signal that does not need phase information.[52] Nevertheless, it accounts for the motion of the wave packet $\psi_B(R, t)$ during the probe−pulse interaction. A detailed analysis, as is given in ref 38, shows that within the

above approximation quantum and classical results are in excellent agreement.

3. Results

3.1. Phase−Energy Picture of I_2 Relaxation. In a previous paper we have shown that a representation of the two-dimensional oscillator distribution function in "energy-phase" coordinates (E, φ) allows for the separation and a subsequent analysis of the energy relaxation and dephasing processes.[40] The transformation from the canonical variables (R, P) to the (E, φ) set of coordinates can be given analytically for the Morse oscillator (well depth D, equilibrium distance R_e, parameter α) as

$$R_E(t) = R_e + \frac{1}{\alpha}\ln\frac{D - \sqrt{DE}\cos(\varphi)}{D - E} \qquad \varphi = \omega_E t \quad (5)$$

This is valid for a particle with energy E, starting at an inner turning point R_0. Furthermore, the above transformation is exact only for an isolated nonrotating oscillator. In all other cases the transformation is approximate and merely serves to elucidate the qualitative picture of vibrational relaxation.

In our former study we treated a restricted phase space of the system: the calculations started with a fixed I−I intramolecular distance and different initial configurations of the ambient gas. In this way, a set of I_2 vibrational trajectories (R, P) were generated which compose the time-dependent oscillator distribution function. A transformation to the phase distribution $\rho(\varphi)$ and energy distribution $\rho(E)$ was then performed using eq 5. In this paper we perform a full simulation of femtosecond pump−probe experiments,[23] therefore the initial distribution of I_2 vibrational coordinates and momenta is prepared according to the pump−laser pulse characteristics (eq 1).

Let us first discuss the case where no collisions occur, i.e., we regard isolated iodine molecules. The energy distribution function in the B state, obtained in the numerical modeling of the excitation process (eq 1), is shown in Figure 2 (lower panel). The finite width of $\rho(E)$ results from the spectral width of the ultrashort pump pulse. Since the dynamics takes place in an anharmonic potential, this distribution generates a dephasing, even in the absence of an environment. Figure 2 (lower curve in upper panel) shows the time evolution of the phase distribution function for cold (0 K) I_2 molecules. The initial phase distribution ($t = 0$ ps) has already some width as a result of the femtosecond pulse excitation. As stated above, the broadening at later times is due to the anharmonicity of the potential.

For molecules having various vibrational frequencies, *a desynchronization* of vibrational motion takes place, therefore an initially localized swarm of classical trajectories disperses as time goes along. This broadening depends on the initial energy distribution only and should be distinguished from a collision-induced dephasing. For a free molecule, a phase distribution at time t can be obtained simply from the energy distribution using the relation $\varphi = \omega_E t$. In a quantum mechanical treatment, the subsequent time evolution yields a vibrational revival at about 18 ps,[8,28] i.e., the dispersed wave packet refocuses. As a consequence, at the time of a revival, the transient signals show the same temporal behavior as for short delay times. Various aspects of this quantum effect, which is well known in quantum optics,[53] have been discussed theoretically.[28,54−57] Also, several experiments on diatomic molecules[7,8,58−61] investigated vibrational revivals. In the classical approximation, the dynamical system has no discrete vibrational levels so that no revival can occur. While for most cases considered in the present work, the relaxation effectively destroys the quantum coherence and revivals, the application of the classical description to the case of isolated molecules is useful to describe the qualitative picture, namely that the oscillators with different energies have different vibrational and rotational periods. It is noteworthy that the short-time evolution is similar for both the quantum and classical systems.[28,54]

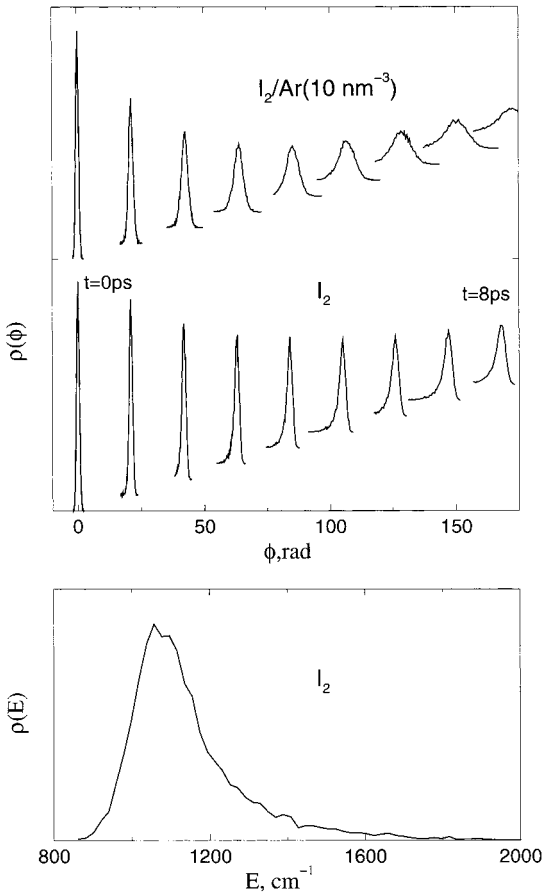

Figure 2. Upper panel: phase distributions $\rho(\varphi, t)$ of I_2 oscillators (0 K) prepared by a 620 nm pump laser pulse. Curves are displayed at different times in intervals of 1 ps. The lower curve shows the collision-free case; the upper curve is obtained in the case of collisions with Ar atoms. The lower panel contains the energy distribution $\rho(E)$ resulting from the pump excitation for noninteracting I_2 molecules.

Obviously, collisions intensify the broadening effect, as can be seen in the upper curve displayed in Figure 2. We show this picture of the phase distribution evolution for an illustration of the collision-induced dephasing effect; quantitative considerations based on the Fourier analysis of the coordinate autocorrelation function are presented in the following subsection.

Figure 3 shows the widths of the phase distribution obtained as a function of time and under different conditions. The widths (fwhm) were estimated by a Gaussian fit to the numerical results. The solid line corresponds to 0 K and the dotted line corresponds to 300 K, both in no environment. A comparison reveals the effect of the rotational motion. Regular oscillations of the vibrational energy resulting from the rovibrational coupling have little impact on the phase. Meanwhile, the overall change in the centrifugal barrier, and thus in the rotational period, leads to an additional phase broadening in the ensemble, as is shown in Figure 3. The dashed line shows a collision-induced phase broadening and corresponds to Figure 2 (upper curve).

3.2. Dephasing and Pump−Probe Signals for I_2/(Ar,He) at Different Pressures. We will now discuss the pressure dependence of pump−probe signals and analyze the corre-

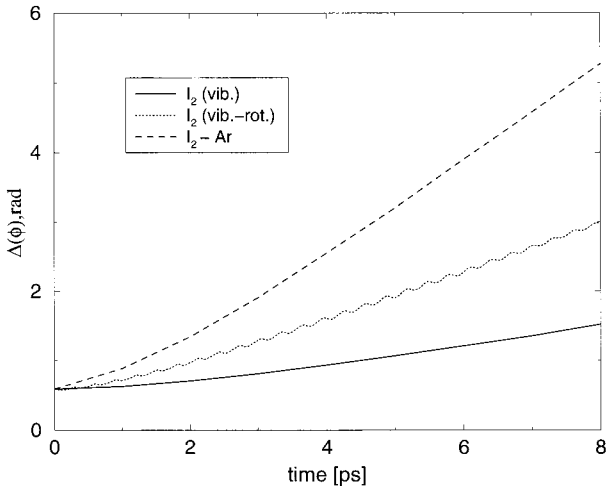

Figure 3. The widths of the phase distribution are plotted as a function of time. Solid line: 0 K, only vibrational motion. The influence of rotations can be seen in the dotted line (300 K). Collisions with Ar at 10 nm^{-3} density and 300 K result in the dashed curve.

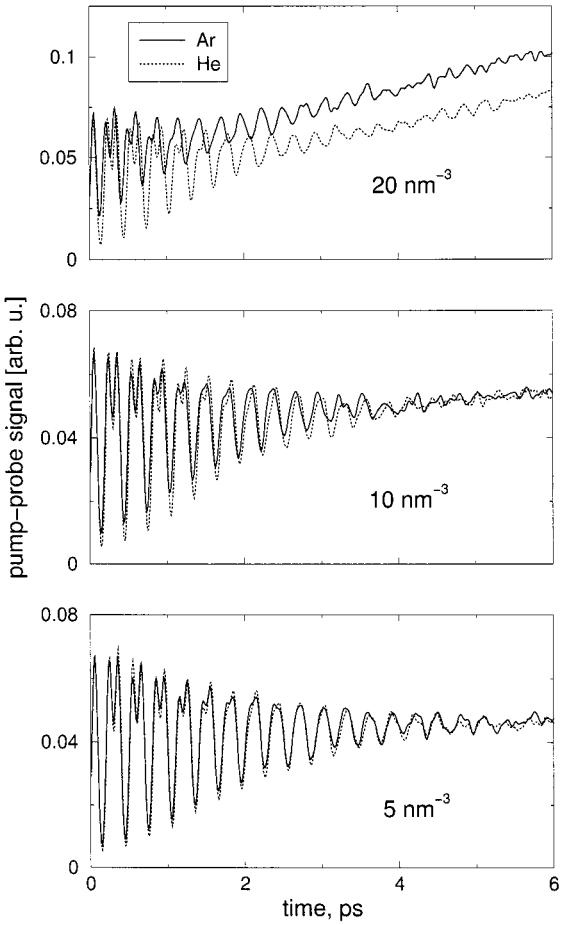

Figure 4. Pump−probe signals (620 nm pump, 280 nm probe) calculated for I_2/Ar (solid line) and I_2/He (dotted line) at different pressures, as indicated.

sponding relaxation processes. Figure 4 shows calculated transients for I_2 embedded in Ar (solid line) and He (dotted line) gases at a temperature of 300 K and different pressures, as indicated. The probe wavelength is set to 280 nm, i.e., the probe pulse monitors the motion of the vibrational wave packet in a window that is spatially well separated from the turning points of the motion, as is indicated in Figure 1 (case (a)). Several trends can be taken from the figure. First of all, the decay of the oscillations in the signals is independent of the solvent mass. This can be explained by the fact that, despite of a smaller momentum transfer during an I_2−He collision compared to the Ar case, the He atoms move faster than Ar so that the collision frequency is larger for He. The dephasing rate is a product of the dephasing resulting from a single collision ($\Delta\phi \sim m\bar{v}$) and the collision rate ($r \sim s^2\bar{v}$). Here m, σ, and $\bar{v}$ are the mass, diameter, and the mean velocity of the solvent atom, respectively. The product is proportional to the temperature and the square of the effective collision diameter and thus does not depend on the solvent mass. The difference in the diameter (estimated from Rg−I equilibrium distances) $\sigma^2_{Ar-I}/\sigma^2_{He-I} \sim 1.1$ is too small to give significant differences in relaxation rates at the same pressure. Naturally, these considerations do not hold any longer in the limit of very high density (see upper panel of Figure 4).

Another interesting effect apparent in Figure 4 is the increase of the transient background signal at longer times if the pressure is sufficiently high. This is due to the fact that the energy relaxation results in I_2 trajectories moving in a more restricted interval around the equilibrium distance, so that the classical orbits are located, in the average, for a longer time within the Franck−Condon window, thus enhancing the signal.[62] Another situation arises if the probe laser wavelength defines a window located at the outer turning point region of the unperturbed wave packet motion, as is indicated by the arrow (c) in Figure 1. In this case, the relaxation results in a decrease of the background signal since the trajectories, with decreasing energy, are no longer able to enter the probing window.

Let us now, in more detail, discuss the decay of the oscillatory structure visible in the calculated transients for the 280 nm probe transition (Figure 4). As was shown before,[40] this behavior is determined completely by the phase distribution broadening and, the dephasing time found from the Fourier transform of the signal is consistent with the time obtained from the coordinate autocorrelation function $C(t) = \langle R(0)R(t)\rangle$, where the brackets denote the ensemble average over all I_2 trajectories. In what follows, we apply this method to analyze the density dependence of the dephasing rate. Therefore we calculated $C(t) = \langle R(0)R(t)\rangle$ for an entire range of He and Ar pressures. The offset and the nonoscillatory decay (which is due to energy relaxation) were eliminated by subtraction of a linear contribution of the form $A - Bt$. The power spectrum $J(\omega) = |\int_0^\infty dt\, \exp(i\omega t)C(t)|^2$ consists of the fundamental peak centered at the I−I vibrational frequency ω_0 and of a number of overtones. The fundamental peak is fitted by a Lorentz contour $1/[(\omega_0 - \omega)^2 + k_2^2]$, where k_2 is the dephasing rate.

The vibrational energy relaxation rate can be calculated as well, using a parametrization of the mean vibrational energy $\langle E\rangle - k_B\mathcal{T}$ with an exponentially decaying function $\exp(-k_1 t)$ (here $\mathcal{T}$ is the ambient gas temperature). Figure 5 shows the vibrational energy relaxation rate k_1 and the dephasing rate k_2 as a function of the Ar and He pressure. Points were calculated each 2.5 nm^{-3}. It is noteworthy that the rate constant k_1 is also independent of the solvent mass for reasons discussed above.

It was already mentioned that the background signals obtained for different probe wavelengths will show different traces of the energy relaxation process. This is documented in Figure 6, which contains transients calculated with three probe−pulse wavelengths for a density of 10 nm^{-3}, corresponding approximately to a pressure of 400 bar. As one can take from Figure 1, a 280 nm probe transition defines a Franck−Condon window somewhere near the equilibrium point, while in the case of 330 nm the window is shifted to the outer turning point

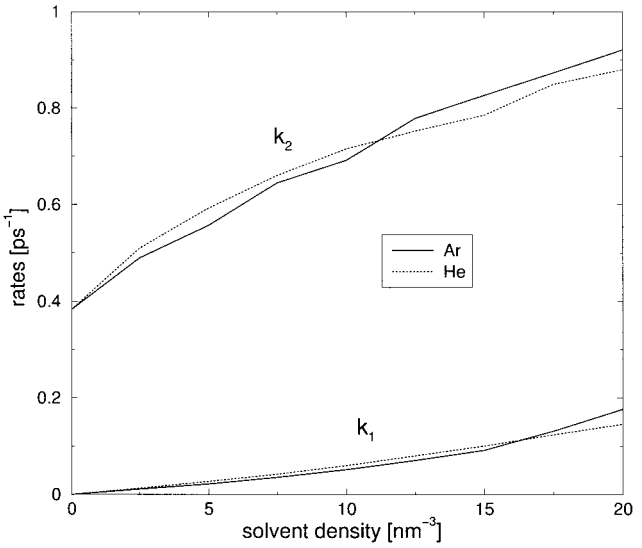

Figure 5. Calculated vibrational relaxation rates (k_1) and dephasing rates (k_2) as a function of the solvent gas pressure.

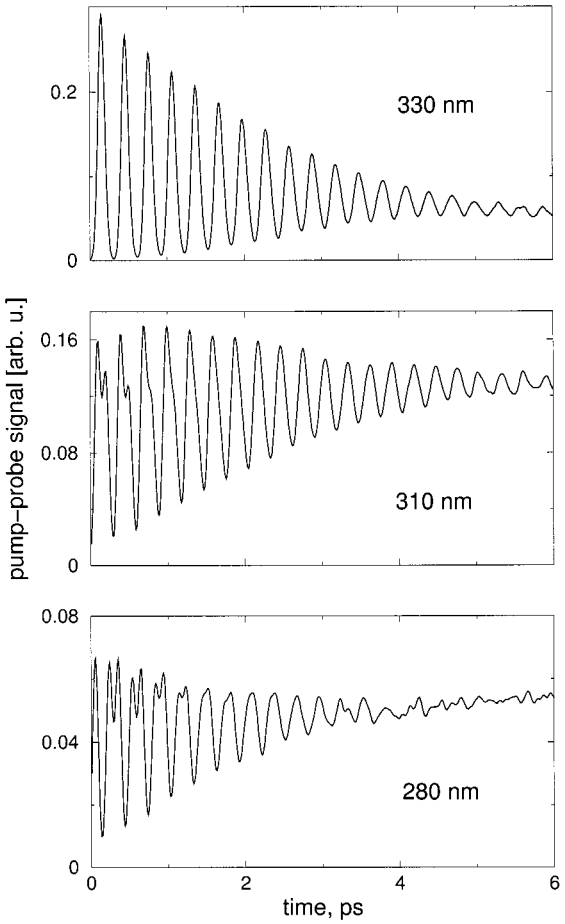

Figure 6. Pump−probe signals for I_2/Ar(10 nm^{-3} density) for different probe−pulse wavelengths, as indicated.

region. The curves displayed in Figure 6 clearly demonstrate that the decay rate for the oscillations depends on the position of the FC window for the probe transition. The collision-induced relaxation of the oscillator energy leads to a variation of the location of the mean outer turning point of the molecular vibrations with respect to the FC window. This dynamical effect leads to a complicated density dependency of the rates k_2 derived from pump−probe signals at different probe laser wavelengths.

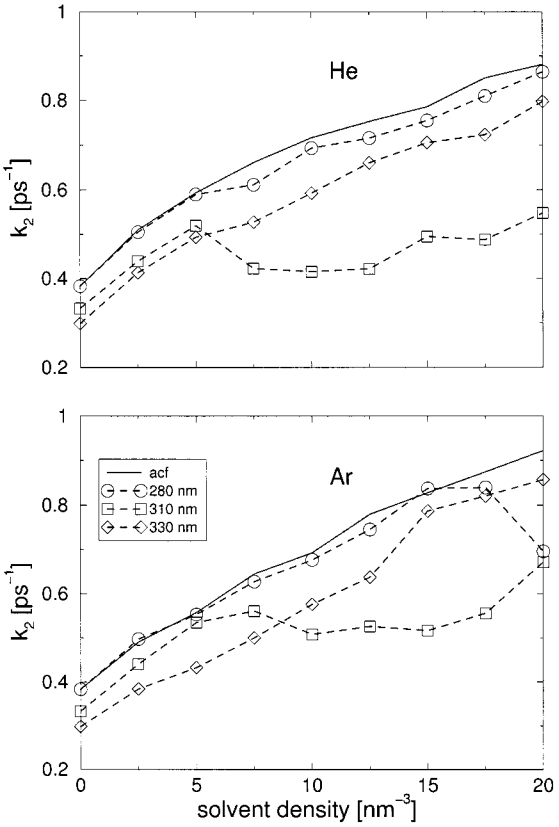

Figure 7. Dephasing rate k_2 calculated from the Fourier transform of the coordinate autocorrelation function (acf, solid line) and pump−probe signals. The latter were obtained for probe wavelengths of 280 nm (circles), 310 nm (squares), and 330 nm (diamonds), respectively.

Figure 7 shows k_2 as a function of the ambient gas density. The solid line shows the dephasing rate obtained from the decay of the coordinate autocorrelation function (acf), whereas the dashed lines correspond to rates obtained from the transient signals for three probe wavelengths, as indicated. An excellent agreement between the rates derived from the acf and from the pump−probe signals, using a 280 nm probe, is observed up to very high pressures. An exception is the 20 nm^{-3} density of Ar gas, at which a rapid energy relaxation influences the signal decay. For other probe−pulse wavelengths and in particular for the 310 nm, as was used in the experiment of Liu et al.,[23] a distinguishable deviation from the values, obtained from the autocorrelation function, is observed.

Discussion and Summary

In a series of pump−probe experiments, Zewail and co-workers have addressed the dephasing process of an initially coherent I_2 ensemble interacting with rare-gas environments.[22,23] In an analysis of the results, they fitted the signals as[23]

$$S(t) = A + B\mathrm{e}^{-k_1 t} + \mathrm{e}^{-k_2 t}\sum_{i=1}^{3} C_i \cos(\omega_i t + \phi_i) \qquad (6)$$

where k_1 is associated with an exponential decay due to predissociation and vibrational relaxation and the rate constant k_2 describes the decay of the oscillatory structure. The sum runs over frequency components that correspond to differences in the eigenenergies of the anharmonic I_2 oscillator.

Let us, in what follows, compare the results of this procedure with our results. In doing so, we have to regard the case where a 310 nm probe pulse is employed. Here a very good agreement

between the rate constants k_2 obtained from our molecular dynamics results and from the fit to the experimental signal is found. This is true for the absolute numbers as well as the pressure dependence as shown in Figure 7. Note however, that this agreement is obtained only in the case of a 310 nm probe excitation. As an important result of our study, the rate constants k_2, as extracted from the coordinate autocorrelation function on one hand and from pump−probe signals on the other, in general deviate from each other. Our numerical results show, that the analysis of pump−probe signals gives the correct values of k_2, if the Franck−Condon window for the probe transition is located close to the equilibrium distance in the intermediate electronic state. The density dependence of the dephasing rate obtained from the autocorrelation function shows a smooth behavior. The plateau occurring at intermediate pressures, as extracted from the experimental (as well as our theoretical) pump−probe signal is the result of a complex interplay between vibrational relaxation and dephasing. It would be interesting to tune the probe laser wavelength to, e.g., 280 nm in order to confirm this theoretically obtained result.

The parametrization given in eq 6 reflects the quantization of the vibrational motion and can reproduce revivals at later times. Fourier transform of the second term appearing in eq 6 gives a Lorentz contour for each frequency component, which all have the same width equal to k_2. Therefore, the relaxation rates obtained with help of the parametrization are consistent with our calculations except for the zero density limit. Our classical approach does not resolve quantum-mechanical vibrational levels and yields a nonzero width for the dephasing rate in the absence of ambient gas. However, this difference completely disappears for pressures above 75 bar (corresponding to 2.0 nm^{-3} density)[23] since collisions with rare-gas atoms destroy the coherence and lead to a merging of the spectral lines into a wide classical-like band. It is worthwhile to stress once more that this band includes both the collision-induced dephasing and the anharmonicity contribution. The separation of the two effects, e.g., with the help of a semiclassical or mixed quantum-classical dynamics, is an interesting problem that is, however, out of the scope of the present study.

We note that the authors of ref 23 have also performed molecular dynamics calculations. The theoretical dephasing rate has been extracted from the coordinate autocorrelation function as $k_2 = 1/\tau_{1/2}$, where $\tau_{1/2}$ is the time when $\langle R(t)R(0)\rangle$ decays to one-half of its initial value. A behavior similar to the experimental observations has been obtained using this method.[23] On the contrary, our calculations yield a slowly changing rate k_2 over the entire considered density range (see Figure 5). The difference between our approach and the one employed in ref 23 is that we use the Fourier analysis of the autocorrelation function and the pump−probe signals to extract the decay rates. For the nonexponential decay of the oscillating function, this method does not suffer from ambiguities related to the decay law.[40]

A good agreement between our calculations and the calculations of ref 23 is achieved in the middle-pressure range for the dephasing rate k_2 and for the vibrational energy decay rate k_1. As for the experimental manifestation of the vibrational energy relaxation, a usual point of view is that the background signal decay is due to both the energy relaxation and predissociation.[24] However, as it was discussed above, the effect of energy relaxation on pump−probe signals is more complex than a simple decay and depends on the probe−pulse wavelength. For example, Figure 6 shows that for 400 bar pressure, the vibrational relaxation does not seem to lead to the decay of the signal calculated with a 310 nm wavelength, rather, a small rise of the signal background is observed. From Figure 6 one can infer that the effect of vibrational relaxation on the background signal is small in comparison with what has been observed experimentally.[22] Therefore, it could be concluded that measurements of the background decay rates yield information about collision-induced predissociation dynamics in I_2.

In summary, we presented a thorough molecular dynamics study of the collision-induced vibrational relaxation in I_2 embedded in rare-gas environments. An analysis of the oscillator distribution-function in "energy-phase" coordinates allows us to separate the vibrational energy relaxation and dephasing processes. A theoretical value of the dephasing rate k_2 can be obtained from the Fourier analysis of the coordinate autocorrelation function, while the energy relaxation rate k_1 is deduced from an exponential fit to the mean oscillator energy. Theoretical values of the rates k_1 and k_2 do not depend on the mass of the solvent gas, confirming predictions of a simple thermodynamic model.

The dephasing effect manifests itself in a decay of the oscillatory structure of pump−probe signals. We showed that the experimental estimate of the dephasing rate with help of pump−probe spectroscopy depends on the probe laser wavelength. By choosing a probe wavelength for which the Franck−Condon window is located far from the outer turning point in the state where the vibrational dynamics takes place, the dephasing rates deduced from the signal are similar to those extracted from the autocorrelation function.

Furthermore, it was demonstrated that, due to the preparation of an energy distribution in the pump process and due to the anharmonicity of the corresponding potential curve, the decay rate of the pump−probe signal contains both the collision-induced and anharmonicity contributions. A careful analysis of experimental signals is required in order to obtain the pure collision-induced contribution. Also, the vibrational energy relaxation manifests itself quite variously in pump−probe signals, depending on the probe-laser wavelength.

Acknowledgment. This work was supported by the Deutsche Forschungsgemeinschaft (Schwerpunktprogramm "Time-dependent phenomena and methods in quantum systems of physics and chemistry") and by the Fonds der Chemischen Industrie. A.K.K. thanks the Deutsche Forschungsgemeinschaft for financial support.

References and Notes

(1) Zewail, A. H. *Femtochemistry*; World Scientific: Singapore, 1994; Vols.1, 2.

(2) *Femtosecond Chemistry*; Manz, J.; Wöste, L., Eds.; VCH: Weinheim, 1995.

(3) *Femtochemistry and Femtobiology*; Sundström, V., Ed.; Imperial College Press: London, 1997.

(4) *Femtochemistry*; Chergui, M., Ed.; World Scientific: Singapore, 1996.

(5) Zewail, A. H. *J. Phys. Chem.* **2000**, *104*, 5660.

(6) Zewail, A. H. *Angew. Chem., Int. Ed. Engl.* **2000**, *39*, 2586.

(7) Bowman, R. M.; Dantus, M.; Zewail, A. H. *Chem. Phys. Lett.* **1989**, *161*, 297.

(8) Gruebele, M.; Zewail, A. H. *J. Chem. Phys.* **1993**, *98*, 883.

(9) Fischer, I.; Villeneuve, D. M.; Vrakking, M. J. J.; Stolow, A. *J. Chem. Phys.* **1995**, *102*, 5566.

(10) Fischer, I.; Vrakking, M. J. J.; Villeneuve, D. M.; Stolow, A. *Chem. Phys.* **1996**, *207*, 331.

(11) Kohler, B.; Yakovlev, V. V.; Che, J.; Krause, J. L.; Messina, M.; Wilson, K. R.; Schwentner, H.; Whitnell, R. M.; Yan, Y. *Phys. Rev. Lett.* **1995**, *74*, 3360.

(12) Stapelfeldt, H.; Constant, E.; Corkum, P. B. *Phys. Rev. Lett.* **1995**, *74*, 3780.

(13) Schmitt, M.; Knopp, G.; Materny, A.; Kiefer, W. *Chem. Phys. Lett.* **1997**, *270*, 9.
(14) Schmitt, M.; Knopp, G.; Materny, A.; Kiefer, W. *J. Phys. Chem. A* **1998**, *102*, 4059.
(15) Larsen, J. J.; Moerkbak, N. J.; Olesen, J.; Bjerre, N.; Machholm, M.; Keiding, S. R.; Stapelfeldt, H. *J. Chem. Phys.* **1998**, *109*, 8857.
(16) Materny, A.; Chen, T.; Schmitt, M.; Siebert, T.; Vierheilig, A.; Engel, V.; Kiefer, W. *Appl. Phys. B* **2000**, *71*, 299.
(17) Lozovoy, V. V.; Grimberg, B. I.; Brown, E. J.; Pastirk, I.; Dantus, M. *J. Raman Spectrosc.* **2000**, *31*, 41.
(18) Warmuth, Ch.; Tortschanoff, A.; Milota, F.; Shapiro, M.; Prior, Y.; Averbukh, I. Sh.; Schleich, W.; Jakubetz, W.; Kauffmann, H. F. *J. Chem. Phys.* **2000**, *112*, 5060.
(19) Zadoyan, R.; Li, Z.; Martens, C. C.; Apkarian, V. A. *J. Chem. Phys.* **1994**, *101*, 6648.
(20) Bargheer, M.; Dietrich, P.; Donovang, K.; Schwentner, N. *J. Chem. Phys.* **1999**, *111*, 8556.
(21) Flachenecker, G.; Behrens, P.; Knopp, G.; Schmitt, M.; Siebert, T.; Vierheilig, A.; Wirnsberger, G.; Materny, A. *J. Phys. Chem. A* **1999**, *103*, 3854.
(22) Lienau, C.; Zewail, A. H. *J. Phys. Chem.* **1996**, *100*, 18629.
(23) Liu, Q.; Wan, C.; Zewail, A. H. *J. Phys. Chem.* **1996**, *100*, 18666.
(24) Materny, A.; Lienau, C.; Zewail, A. H. *J. Phys. Chem.* **1996**, *100*, 18650.
(25) Franck, J.; Rabinowitch, E. *Trans. Faraday Soc.* **1934**, *30*, 120.
(26) Wan, C.; Gupta, M.; Baskin, J. S.; Kim, Z. H.; Zewail, A. H. *J. Chem. Phys.* **1997**, *106*, 4353.
(27) Manz, J.; *Nobel Symposium 101*; Imperial College Press: London, 1997; pp 80−318.
(28) Ermoshin, V. A.; Kazansky, A. K.; Engel, V. *J. Chem. Phys.* **1999**, *111*, 7807.
(29) Li, Z.; Fang, J.-Y.; Martens, C. C. *J. Chem. Phys.* **1996**, *104*, 6919.
(30) Che, J.; Zhang, W.; Yan, Y. J. *J. Chem. Phys.* **1997**, *106*, 6947.
(31) Shen, Y.-C.; Cina, J. A. *J. Chem. Phys.* **1999**, *110*, 9793.
(32) Whitnell, R. M.; Wilson, K. R.; Yan, Y., Zewail, A. H. *J. Mol. Liq.* **1994**, *61*, 153.
(33) Walkup, R. E.; Misewich, J. A.; Glownia, J. H.; Sorokin, P. P. *J. Chem. Phys.* **1991**, *94*, 3389.
(34) Fried L. E.; Mukamel, S. *J. Chem. Phys.* **1990**, *93*, 3063.
(35) Hartmann, M.; Pittner, J.; Bonacic-Koutecky, V.; Heidenreich, A.; Jortner, J. *J. Chem. Phys.* **1998**, *108*, 3096.
(36) Andrianov, I.; Bonacic-Koutecky, V.; Hartmann, M.; Manz, J.; Pittner, J.; Sundermann, K. *Chem. Phys. Lett.* **2000**, *318*, 256.
(37) Mukamel, S. *Principles of Nonlinear Optical Spectroscopy*; Oxford University Press: New York, 1995.
(38) Ermoshin, V. A.; Engel, V. *Euro. Phys. J. D*, in press.
(39) Dahl, J. P. In *Conceptual Trends in Quantum Chemistry*; Kryachko, E. S., Calais, J. L., Eds.; Kluwer: Dordrecht, 1994; pp 199−226.
(40) Kazansky, A. K.; Ermoshin, V. A.; Engel, V. *J. Chem. Phys.* **2000**, *113*, 8865.
(41) Allen, M. P.; Tildesley, D. J. *Computer Simulations of Liquids*; Oxford University Press: Oxford, 1989.
(42) Fang, J.-Y.; Martens, C. C. *J. Chem. Phys.* **1996**, *105*, 9072.
(43) Perrot, J. P.; Bouvier, A. J.; Bouvier, A.; Femelat, B.; Chevaleyre, J. *J. Mol. Spectrosc.* **1985**, *114*, 60.
(44) Garcia-Vela, A.; Villarreal, P.; Delgado-Barrio, G. *J. Chem. Phys.* **1990**, *92*, 6504.
(45) Gray, S. K. *Chem. Phys. Lett.* **1992**, *197*, 86.
(46) Aziz, R. A.; Janzen, A. R.; Moldover, M. R. *Phys. Rev. Lett.* **1995**, *74*, 1586.
(47) Aziz, R. A.; Chen, H. H. *J. Chem. Phys.* **1977**, *67*, 5719.
(48) Lax, M. *J. Chem. Phys.* **1952**, *20*, 1752.
(49) Hiller, E. M.; Cina, J. A. *J. Chem. Phys.* **1996**, *105*, 3419.
(50) Braun, M.; Meier, C.; Engel, V. *J. Chem. Phys.* **1995**, *103*, 7907.
(51) Meier, C.; Engel, V. In *Femtosecond Chemistry*; Manz, J.; Wöste, L., Eds.; VCH: Weinheim, 1995; Chapter 11.
(52) Dietz, H.; Engel, V. *J. Phys. Chem. A* **1998**, *102*, 7406.
(53) Eberly, J. H.; Narozhny, N. B.; Sanchez-Mondragon, J. J. *Phys. Rev. Lett.* **1980**, *44*, 1323.
(54) Averbukh, I. Sh.; Perel'man, N. F. *Phys. Lett. A* **1989**, *139*, 449.
(55) Knospe, O.; Schmidt, R. *Phys. Rev. A* **1996**, *54*, 1154.
(56) Leichtle, C.; Averbukh, I. Sh.; Schleich, W. P. *Phys. Rev. Lett.* **1996**, *77*, 3999.
(57) Leichtle, C.; Averbukh, I. Sh.; Schleich, W. P. *Phys. Rev. A* **1996**, *54*, 5299.
(58) Bowman, R. M.; Dantus, M.; Zewail, A. H. *Chem. Phys. Lett.* **1989**, *161*, 297.
(59) Baumert, T.; Engel, V.; Röttgermann, C.; Strunz, W. T.; Gerber, G. *Chem. Phys. Lett.* **1992**, *191*, 639.
(60) Vrakking, M. J. J.; Villeneuve, D. M.; Stolow, A. *Phys. Rev. A* **1996**, *54*, R37.
(61) Averbukh, I. Sh.; Vrakking, M. J. J.; Villeneuve, D. M.; Stolow, A. *Phys. Rev. Lett.* **1996**, *77*, 3518.
(62) Ermoshin, V. A.; Flachenecker, G.; Materny, A.; Engel, V. *Chem. Phys. Lett.* **1999**, *311*, 146.